Published in final edited form as:
Integr Biol (Camb). 2011 June 6; 3(6): 663–674. doi:10.1039/c0ib00156b.

Measurement and analysis of traction force dynamics in response to vasoactive agonists

Michael T. Yang[1], **Daniel H. Reich**[2], and **Christopher S. Chen**[1]

[1] Department of Bioengineering, University of Pennsylvania, Philadelphia, PA

[2] Department of Physics and Astronomy, Johns Hopkins University, Baltimore, MD

Abstract

Mechanical traction forces exerted by adherent cells on their surroundings serve an important role in a multitude of cellular and physiological processes including cell motility and multicellular rearrangements. For endothelial cells, contraction also provides a means to disrupt cell-cell junctions during inflammation to increase permeability between blood and interstitial tissue compartments. The degree of contractility exhibited by endothelial cells is influenced by numerous soluble factors, such as thrombin, histamine, lysophosphatidic acid, sphingosine-1-phosphate, and vascular endothelial growth factor (VEGF). Upon binding to cell surface receptors, these agents trigger changes in cytoskeletal organization, adhesion and myosin II activity to varying degrees. While conventional antibody-based biochemical assays are suitable for detecting relatively large changes in biomarkers of contractility in endpoint format, they cannot resolve subtle or rapid changes in contractility and cannot do so noninvasively. To overcome these limitations, we developed an approach to measure the contractile response of single cells exposed to contractility agonists with high spatiotemporal resolution. A previously developed traction force sensor, comprised of dense arrays of elastomeric microposts on which cells are cultured, was combined with custom, semi-automated software developed here to extract strain energy measurements from thousands of time-lapse images of micropost arrays deformed by adherent cells. Using this approach we corroborated the differential effects of known agonists of contractility and characterized the dynamics of their effects. All of these agonists produced a characteristic first-order rise and plateau in forces, except VEGF, which stimulated an early transient spike in strain energy followed by a sustained increase. This novel, two-phase contractile response was present in a subpopulation of cells, was mediated through both VEGFR2 and ROCK activation, and its magnitude was modulated by receptor internalization. Interestingly, the concentration of VEGF could shift the proportion of cells that responded with a spike versus only a gradual increase in forces. Furthermore, cells repeatedly exposed to VEGF were found to contract with different dynamics after pretreatment, suggesting that exposure history can impact the mechanical response. These studies highlight the importance of direct measures of traction force dynamics as a tool for studies of mechanotransduction.

Key terms

Traction force; stress fiber; myosin; micropost array; VEGF

Correspondence: Christopher S. Chen, 510 Skirkanich Hall, 210 S. 33rd Street, Philadelphia, PA 19104, chrischen@seas.upenn.edu, 215-746-1754 (phone), 215-746-1752 (fax).

Introduction

Physical forces generated by cells regulate a diverse array of cellular functions such as migration, proliferation, differentiation and gene expression [1–5]. These cellular forces arise from cross-bridging interactions between myosin II motors and the actin cytoskeleton, and are transmitted through focal adhesions to the external extracellular matrix as traction forces [6, 7]. The regulation of contractility is a complex process that involves the integration of outside-in and inside-out signals between cells and their microenvironment [8–10]. Although intense efforts have been directed towards understanding how internal forces, external insoluble cues such as substrate stiffness and ligand density, and adhesion-mediated signaling cooperate to regulate cellular phenotype, the role soluble factors play in regulating contractility has not been investigated as extensively [11–17].

For instance, a host of soluble vasoactive substances have been implicated in endothelial barrier function through their effects on cytoskeletal organization and contractility [18]. The best characterized vasoactive agent has been thrombin, a potent coagulation protein that also activates platelets. Thrombin strongly increases endothelial contractility by activating RhoA and its effector, Rho kinase (ROCK) as well as myosin light chain kinase (MLCK), leading to a dramatic increase in the phosphorylation of myosin light chain 2 (MLC), and therefore myosin II motor activity [19–24]. This increase in contractility leads to breakage of cell-cell junctions and loss of endothelial barrier integrity [25]. Lysophosphatidic acid (LPA) and sphingosine-1-phosphate (S1P), which are released by activated platelets, and histamine also increase contractility through similar mechanisms as thrombin, but differ in the relative degree and duration of activation of Rho, MLCK, and a Rho-related GTPase, Rac [20, 24–31]. Although it has largely been accepted that the contractile response is a central component of the vasoactivity of all of these agents, contractile responses have not yet been systematically documented.

In addition to molecules specifically associated with endothelial barrier function, many growth factors also have some cytoskeletal effects. For example, vascular endothelial growth factor (VEGF) is best known for its role in promoting angiogenesis, but it also can increase vascular permeability [32]. Like other vasoactive agents, VEGF induces the formation of stress fibers and focal adhesions in endothelial cells [33]. However, this has been attributed to Rac activation and not Rho [33]. Moreover, VEGF signaling has not been explicitly linked to changes in myosin activity nor has direct measurement of the presence or absence of a contractile response to VEGF been reported [34–37].

Here, we describe a method to measure the dynamic contractile responses of cells exposed to different soluble factors. This method is based on a previously developed microfabricated substrate comprised of arrays of closely spaced, vertical elastomeric microposts capable of measuring nanonewton-scale traction forces [15, 16, 38]. We adapted this platform to image multiple cells with high spatiotemporal resolution, and used it to track the contractility dynamics of hundreds of individual endothelial cells before and after stimulation with a set of vasoactive soluble factors. Using this high-throughput system, we show that all of the abovementioned vasoactive compounds impact cellular contractility, though with slightly different dynamics and magnitudes. VEGF, in particular, elicited a relatively unique contractile response that was undetectable by conventional biochemical methods. Using hierarchical clustering to analyze the temporal profiles of the heterogeneous contractile responses of single cells, we extracted a robust two-phase contractile response to VEGF. This novel observation demonstrates the utility of dynamic traction force imaging for examining the mechanisms regulating contractility.

Results

In adherent cells cultured on rigid substrata, isometric tension promotes the assembly of actin filaments into thick bundles known as stress fibers [6]. Myosin II-driven movement of actin filaments is the primary driving force in these cytoskeletal rearrangements [39]. Moreover, biphosphorylation of MLC catalyzes the ATPase activity of myosin II and is the most direct biochemical marker of myosin II activation [40]. To screen the effects of different soluble factors on contractility, human umbilical vein endothelial cells (HUVECs) were cultured on fibronectin-coated rigid substrata, exposed to soluble factors for durations of 10 and 30 minutes and then fixed and immunostained for F-actin stress fibers and phosphorylated MLC (ppMLC). Qualitatively, histamine, LPA, S1P, serum, thrombin and VEGF all stimulated actin stress fiber formation compared to the bovine serum albumin (BSA) treatment control (Fig. 1a). The averaged intensities of ppMLC within individual cells indicate that thrombin, LPA, S1P and serum, but not histamine and VEGF, significantly increase ppMLC levels (Fig. 1b). This result was confirmed by immunoblotting for ppMLC and MLC in cell lysates following the same treatment conditions (Fig. 1c). Despite their weak effects on ppMLC levels, histamine and VEGF caused significant increases in actin polymerization (Fig. 1d). Furthermore, cells treated with histamine exhibited significantly more stress fibers than cells treated with more potent agonists such as LPA and S1P. These observations not only suggest that these soluble factors might differentially increase contractility, but that myosin phosphorylation may not be ideally suited to detect the effects of some agonists. Furthermore, since both assays are endpoint assays, there is always a concern that differences in the dynamics of contractility could be overlooked.

To address these concerns, we utilized elastomeric micropost array substrates (mPADs) to examine directly the effects of these soluble factors on contractility. Cells cultured atop these arrays are able to transmit traction forces that cause the underlying microposts to deflect [15, 16, 38]. By multiplying these deflections by the spring constant for the microposts and integrating over the magnitudes of the deflections, the strain energy or contractile work generated by the cell can be quantified. While we have previously used mPADs for steady-state measurements of contractility, in this study we introduced additional capabilities to allow for analysis of rapid changes in cellular tractions. A custom, semi-automated program was developed to quantify traction forces from large stacks of time-lapse images in a timely manner. This was coupled with a motorized microscope stage for tracking multiple cells simultaneously, allowing us to observe and measure the contractility dynamics of cells before and after exposure to a wide array of treatment conditions.

To test the sensitivity of this approach for reporting rapid changes in contractility, we stimulated quiescent, green fluorescent protein (GFP)-expressing HUVECs on mPADs with LPA, S1P, histamine and thrombin (Fig. 2). All four agonists elicited a step-like increase in strain energy within 1 minute, with the peak generally occurring 10 minutes after stimulation (Fig. 2b–e). The strongest increases in strain energy within cells were spatially localized primarily to the cell periphery and to microposts already experiencing higher baseline forces before stimulation (Fig. S1). The magnitude of the increase in strain energy was greatest with thrombin, intermediate with LPA and S1P, and smallest with histamine. After reaching the peak magnitude, the average strain energy dropped off to varying degrees for each stimulus. Thrombin-stimulated cells experienced a precipitous decrease in measured strain energy from peak levels, due to the fact that cells rounded up within 12 minutes of stimulation and detached from a significant number of microposts (Fig. S2). A fraction of cells treated with S1P also rounded up, which accounts for the moderate drop-off in strain energy for that treatment condition. In contrast, cells stimulated with LPA or histamine did not round up, and this correlated with only slight drop-offs in average strain

energy from the peak levels. These observations suggest that, while changes in strain energy generally agree with changes in ppMLC level, the two metrics are not always equivalent, especially when changes in cell adhesion alter strain energy but not ppMLC levels.

Having demonstrated the ability of the mPADs to detect differences in the cellular responses to known agonists of contractility, we subsequently investigated the effects of VEGF on contractility. VEGF also induced spatially localized increases in contractility similar to the other agonists (Fig. S1). However, in contrast to the other agonists, VEGF elicited a transient increase, or spike, in strain energy within 5 minutes of stimulation, followed by a brief relaxation, and then a more sustained increase (Fig. 3a). By comparison, cells treated with BSA experienced no significant change in average strain energy. Analysis of variance of the basal strain energies of cells collected from six experiments revealed that almost 90% of the variability is due to differences between individual cells and not between experiments (Table S3). As such, we used statistical analysis to examine changes in contractility within each cell over time, and found that a greater percentage of cells stimulated with VEGF instead of BSA experienced significant increases in strain energy at early, intermediate and late time points in the 30 minutes following stimulation (Fig. 3b). The small fraction of cells treated with BSA that exhibit significant changes in strain energy reveals the inherent noise in single-cell measurements.

Although a typical cell stimulated with BSA showed no change in strain energy, cells stimulated with VEGF either exhibited an early spike, a late sustained increase, or both contractility phenotypes (Fig. 4, Fig. 5a). To determine the distribution of these phenotypes among the observed cells, we used hierarchical clustering to group together cells that displayed similar strain energy profiles [41]. 85 cells exposed to VEGF were clustered based on the shape of the strain energy profiles within the first 10 minutes of stimulation (Fig. 5b). As expected, the majority of cells separated into two groups featuring the two dominant contractility phenotypes. Approximately 30 percent of the cells experienced only a gradual increase in strain energy while nearly 50 percent of the cells rapidly spiked after VEGF stimulation (Fig. 5c and d). Neither of these clusters emerged when the same analysis was applied to cells stimulated with BSA (Fig. S4). Moreover, the robustness of these two contractility phenotypes is conserved across cells with different basal contractile states and spread areas (Fig. 5e–f). Interestingly, this heterogeneity in contractile response was unique to VEGF stimulation, as stimulation by all other agonists led to uniform increases in contractility across all cells. Synchronizing cells to G0 of the cell cycle to achieve a more homogeneous cell population did not reduce the heterogeneity of the contractile responses. Thus, the heterogeneity was not a result of cell to cell differences in the force-generating components.

Recent findings have shown that phosphorylation and internalization of VEGF receptor 2 (VEGFR2) appear to peak around 5 minutes following VEGF stimulation, which correlates with the occurrence of the contractility spikes [42, 43]. Moreover, blocking VEGFR2 internalization with the dynamin inhibitor, Dynasore, was found to not completely block phosphorylation of VEGFR2 after 5 minutes of VEGF stimulation, but did so for longer periods of stimulation [43]. Therefore, it is possible that the dynamics of the contractile response correlate with initial phosphorylation of VEGFR2, receptor internalization, and sustained signaling from within the cell. To address this hypothesis, we applied pharmacological inhibitors to different molecular targets and then stimulated cells with VEGF. Inhibition of VEGFR2 with 10 μM Ki8751 appeared to ablate the contractile response to VEGF, but did not decrease the basal contractility (Fig. 6a). Furthermore, inhibition of ROCK with 25 μM Y-27632 also blocked the VEGF-induced contractility spike and essentially reduced basal contractility to the level of noise in the mPADs measurement (Fig. 6b). Disruption of VEGFR2 internalization with 30–50 μM Dynasore

reduced both the basal contractility and magnitude of the average contractile response, but did not ablate the occurrence of contractile spikes in a fraction of the observed cells (Fig. 6c). These data suggest that VEGFR2 phosphorylation and ROCK-mediated myosin II contraction are necessary to recapitulate both phases of the contractile response, and that receptor internalization may modulate the strength the contractile response. Inspired by these observations, we administered VEGF concentrations ranging from 1 to 100 ng/mL to determine if the strength of the contractile response varied as a function of VEGF concentration. Interestingly, we observed that the proportion of cells experiencing contractility spikes was highest at the highest concentrations of VEGF, whereas gradual increases in contractility were most prevalent at intermediate VEGF levels and non-responsive cells predominated at low VEGF levels. A greater proportion of cells experienced contractility spikes as VEGF concentration was increased from 50 to 100 ng/mL (Fig. 7). In contrast, decreasing VEGF concentration to 10 ng/mL or less resulted in cells exhibiting either a sustained increase in contractility without spiking or no response at all. These data reveal that the two contractile responses computationally extracted earlier (spikes and gradual increases) are differentially accessed by the concentration of VEGF.

As a non-invasive tool, the mPADs is particularly useful for experiments in which a treatment condition is administered repeatedly to examine the effect of treatment history on an output. Here, we assessed how cells responded to repeated VEGF stimulation, by challenging cells with either BSA or VEGF, waiting several hours and then following up with a second dose of VEGF. Interestingly, the majority of cells that initiated a contractile spike after one dose of VEGF did not respond in kind after a second dose of VEGF (Fig. 8a–b). In contrast, when cells were first stimulated with BSA, more than half of the cells initiated a contractile spike after the subsequent addition of VEGF (Fig. 8a,c). Although the sample size is small, this result suggests that the contractile response to VEGF depends on the history of the cells' exposure to stimuli.

Discussion

In this study, we set out to investigate whether different vasoactive soluble factors produced differential effects on cellular contractility. We examined the effects of different stimuli on MLC phosphorylation and stress fiber formation and observed significant differences in how these stimuli regulate these indirect biomarkers of contractility. While thrombin, LPA, S1P and serum were consistently strong promoters of MLC phosphorylation and stress fiber formation, histamine and VEGF had significant effects only on stress fiber formation. Contractility measurements of cells on mPADs that were exposed to LPA, S1P, histamine and thrombin corroborated the measured MLC phosphorylation levels, indicating that strain energy is an accurate analog of biochemical markers of contractility, though with the added benefits of single-cell time-resolved measurements, and non-destructive observation.

Furthermore, we used mPADs to show that VEGF, which does not elicit detectable changes in MLC phosphorylation, does indeed increase cellular contractility. By exploiting the ability of the mPADs to detect small changes in strain energy with high temporal resolution, we observed an averaged, two-phase contractile response of cells to VEGF in which strain energy transiently increased 5 minutes after addition of VEGF, decreased briefly, and then gradually increased again. Although individual cellular responses to VEGF were heterogeneous, cluster analysis showed that the two phases of strain energy increase occurred with great frequency, sometimes in the same cells and sometimes in different cells.

Using pharmacological inhibitors, we show that the contractile response to VEGF is initiated by activation of VEGFR2 and ROCK, and may be modulated by receptor internalization. Although the underlying mechanisms for the two phases of the contractile response are

unclear, a number of studies show possible correlations on the same time scale. One study that examined the role of VE-cadherin in controlling VEGFR2 internalization, found that internalization is greatest between 5–10 minutes after VEGF stimulation [42]. When VE-cadherin is not engaged at junctions, as was the case with our single-cell studies, VEGFR2 is internalized more rapidly and remains in endosomal compartments longer [42]. Moreover, actomyosin-driven contractility has been implicated in integrin endocytosis, and it is known that VEGFR2 associates with the integrin $\alpha_v\beta_3$ after VEGF ligand binding [44–46]. Physiologically, these rapid processes might explain why monolayers of endothelial cells transiently decrease in permeability on the same time scale in response to VEGF, before increasing in permeability for hours [47]. With regards to the observation of fewer spikes in cells after a second stimulation with VEGF, it is possible that exposure to VEGF affects the response to subsequent exposures by altering the distribution and expression of receptors in cells. The observation of a bimodal contractile response to different concentrations of VEGF suggests that sensitivity to VEGF signaling is a critical determinant of the contractile response phenotype. Further studies are necessary to determine if cell to cell heterogeneity in sensitivity to VEGF is due to natural variability in the population or is a functional difference that defines distinct roles for endothelial subpopulations to VEGF stimulation.

In summary, we adapted the mPADs for the study of single-cell contractility dynamics and gained insights into the heterogeneity of cellular responses that could not be captured by other methods. Future development of this technique through improvements in traction force analysis automation and image acquisition capacity will accelerate the screening of greater numbers of treatment conditions, such as different soluble factors, adhesive ligands, inhibitors or matrix rigidities.

Materials and Methods

Cell Culture and Reagents

Human umbilical vein endothelial cells (HUVECs, Lonza, Basel, Switzerland) were cultured in EGM-2 complete medium (Lonza) on gelatin-coated plates. Serum-free EBM-2 (Lonza) was used for starvation steps in all experiments. For live-cell imaging experiments, cells were infected with recombinant adenovirus encoding GFP for 6 hours prior to re-plating onto other substrates for further experimentation. BSA (Sigma, St. Louis, MO), FBS (Invitrogen, Carlsbad, CA), LPA (Avanti Polar Lipids, Alabaster, Alabama), S1P (Sigma), histamine (Sigma), thrombin (Enzyme Research Lab, South Bend, IN), VEGF (R&D Systems, Minneapolis, MN), Ki8751 (EMD Chemicals, Gibbstown, NJ), Y-27632 (Tocris Bioscience, Ellisville, MO), Dynasore (Tocris), and DMSO (Sigma) were reconstituted as per vendor's guidelines for use in experiments.

Substrate Preparation

Elastomeric micropost array substrates (mPADs) were fabricated via polydimethylsiloxane (PDMS; Sylgard 184, Dow-Corning, Midland, MI)-based replica-molding as previously described [38]. Briefly, PDMS prepolymer was poured over a template consisting of silicon microposts, cured at 110°C for 15 minutes and peeled to yield negative molds. Negative molds were silanized with (tridecafluoro-1,1,2,2,-tetrahydrooctyl)-1-trichlorosilane (United Chemical Technologies, Bristol, PA) overnight to aid subsequent release of PDMS cast from the negative molds. PDMS prepolymer was poured over the silanized negative molds and sandwiched against No. 1 coverslips to provide mechanical support. After curing the PDMS at 110°C for 20 hours, the negative molds were peeled off to yield micropost arrays attached to glass. Micropost arrays that were collapsed onto each other were rescued by sonicating the substrates in ethanol for 1 minute and then replacing the ethanol with supercritical CO_2 in a critical point drier (Samdri PVT-3D, Tousimis, Rockville, MD). The microposts used in

this study have a diameter of 1.83 μm, a height of 8.3 μm, and a center-to-center spacing of 4 μm. For live-cell mPADs experiments, mPADs coverslips were mounted onto Mattek dishes (Mattek Corportation, Ashland, MA) using UV-curable adhesive (Norland 68, Norland Products, Cranbury, NJ). The tips of the microposts were then coated with fibronectin (BD Biosciences, San Jose, CA) via microcontact printing. mPADs were fluorescently labeled with 5 μg/ml Δ^9-DiI (1,1′-dioleyl-3,3,3′,3′-tetramethylindocarbocyanine methanesulfonate; Invitrogen). To restrict cell adhesion to only the tips of the microposts, uncoated regions were blocked with 0.2% Pluronics F127 (BASF, Mount Olive, NJ). For non-mPADs experiments, glass coverslips that had been coated with a thin layer of PDMS were uniformly coated with fibronectin (50 μg/mL) for 1 hour. Similarly, 6-well tissue culture plates were coated with PDMS and uniformly coated with fibronectin (25 μg/mL) for 1 hour.

Immunofluorescence Imaging

F-actin reorganization and MLC phosphorylation in response to soluble factor stimulation were assessed by labeling fixed cells with fluorophore-conjugated phalloidin (Invitrogen) and antibody for phospho-myosin light chain 2 (Thr18/Ser19) (ppMLC; Cell Signaling Technology, Beverly, MA), respectively. HUVECs were first plated on fibronectin-coated PDMS coverslips and allowed to spread overnight in EGM-2. The cells were then starved for 4 hours in EBM-2 and stimulated with BSA, histamine, LPA, S1P, serum, thrombin, or VEGF. After 10 and 30 minutes of stimulation, cells were fixed in 3.7% paraformaldehyde (Electron Microscopy Sciences, Hatfield, PA), washed in PBS, permeabilized with 0.1% Triton X-100 (Sigma), blocked with 33% goat serum in PBS, incubated with primary antibodies for ppMLC, washed in PBS, incubated with fluorophore-conjugated phalloidin, secondary antibodies and DAPI nucleic acid stain (Invitrogen), washed in PBS, and finally mounted on glass slides with Fluoromount-G (Electron Microscopy Science). Fluorescent images were acquired at 63x (Plan-Apochromat 63x oil/1.40 NA) on an Axiovert 200M (Zeiss MicroImaging, Thornwood, NY).

Quantification of MLC Phosphorylation

For immunofluorescent images of ppMLC, the average background intensity was subtracted from the intensity within the cell boundary. The adjusted intensity was then divided by cell area and averaged across all cells for each treatment condition. MLC phosphorylation was also assessed by immunoblotting for ppMLC and normalizing against total MLC. HUVECs were cultured on fibronectin-coated PDMS 6-well plates at 1×10^4 cells/cm^2 and allowed to spread overnight in EGM-2. Cells were then starved for 4 hours in EBM-2 and stimulated with BSA, histamine, LPA, S1P, serum, thrombin, or VEGF. After 10 and 30 minutes of stimulation, cells were lysed in Laemmli buffer (Bio-Rad, Hercules, CA). The lysates were run on NuPage 4–12% Bis-Tris gels (Invitrogen) and then transferred onto Immobilon-FL PVDF membranes (Millipore, Billerica, MA). Membranes were simultaneously incubated with antibodies for myosin (light chains 20 kDa) (Sigma) and ppMLC followed by incubation with IRDye-conjugated IgG antibodies (Li-Cor, Lincoln, Nebraska). ppMLC and MLC blotting were subsequently imaged with the Odyssey Infrared Imaging System (Li-Cor).

Quantification of Stress Fiber Formation

Phalloidin-labeled F-actin, which consists primarily of stress fibers and to a lesser extent, lamellipodial and filopodial actin, was segmented using a custom automated image analysis algorithm written in MATLAB (Mathworks, Natick, MA) to produce a binary mask of the phalloidin image. The pixels in the mask were then summed and divided by the cell area to determine the fractional coverage of F-actin, which is averaged across all cells in each

treatment condition. The algorithm uses a series of elongated Laplacian of Gaussian (eLoG) kernels to detect edges in the phalloidin images [48]. *n* anisotropic Gaussians of the form

$$G=\frac{1}{2\pi\sigma_x\sigma_y}e^{-(\frac{x^2}{2\sigma_x}+\frac{y^2}{2\sigma_y})}$$

were generated for each combination of σ_x and σ_y. Each Gaussian is rotated in steps of π/n from 0 to $\pi - \pi/n$, with $n = 15$ for this analysis. The Gaussian kernels are then convolved with the Laplacian filter,

$$\begin{bmatrix} 0 & -1 & 0 \\ -1 & 4 & -1 \\ 0 & -1 & 0 \end{bmatrix}$$

to yield *n* eLoG kernels. Multiple values for σ_x and σ_y were used to detect stress fibers of different thicknesses. The eLoG kernels were convolved with the phalloidin images to produce one response image for each kernel. A single maximum response image was created from this stack of response images, containing the maximum values across all response images at each xy pixel position. This maximum image is then thresholded using the Otsu method to yield the binary mask of the segmented stress fibers [49]. Lastly, round bodies smaller than 78.5 pixels were removed to reduce the contribution of non-filamentous actin clusters.

Live Cell Imaging of Cellular Contractility

To assess the effects of different soluble factors on contractility, HUVECs expressing GFP were seeded onto mPADs overnight and imaged at 20x (Plan-Apochromat 20x/0.8 NA) or 40x (Plan-Neofluar 40x oil/1.30 NA) on an Axiovert 200M, equipped with a temperature and CO_2-controlled cage incubator (In Vivo Scientific, St. Louis, MO) and motorized XY stage. Cells on mPADs were first starved in EBM-2 for 4 hours to reduce their contractile states to basal levels. Individual cells were then identified by GFP and tracked by Axiovision software (Zeiss MicroImaging). For each cell, a fluorescent “base post” image of the DiI-labeled microposts was acquired at a focal plane approximately 1 μm above the base of the microposts. Fluorescent “tip post” and “cell” images of the microposts and GFP, respectively, were then collected at 1 or 3 minute intervals, at a focal plane passing through the tips of the microposts. All images were taken with 1×1 binning to obtain the highest resolution. Small XY translational shifts caused by vibrations during movement of the motorized stage are automatically corrected during image analysis. Focus drift in the Z-axis was infrequent but manually corrected for when encountered. The quality of the high-throughput time-lapse images is therefore equivalent to that of snapshot images. Each time-lapse series consisted of a 15-minute period in which the basal contractility of the cell was observed, followed by addition of a soluble factor and then at least 30 more minutes of observation. Soluble factors were gently mixed with the EBM-2 using a micropipette to minimize disturbances to the microscope setup. For experiments in which pharmacological inhibitors were used, drugs were added between 30 to 60 minutes prior to the addition of the soluble factor.

Strain Energy Quantification

Quantitative analysis of subcellular level strain energies was performed as previously described with software modifications to increase throughput [13, 38, 50]. Briefly, the "base post" image and time series of "tip post" images acquired for each cell were processed with a custom-developed MATLAB program (Mathworks). The centroids of the microposts at the base and tip, representing the undeflected and deflected positions, respectively, were automatically determined by localized binary thresholding and two-dimensional Gaussian curve fitting. Then two semi-automatic detection schemes were used to determine which microposts are attached to the cell. First, the tip and base centroids were registered by minimizing differences in the tip and base positions of a few user-defined "free" microposts that are not attached to cells. Registration reveals which microposts are deflected above an arbitrary threshold of 0.8 pixels. These deflected microposts are flagged as being "attached" to the cell and the strain energies on these microposts constitute the majority of the cellular contractile response. The arbitrary threshold for deflection can be decreased but will increase the number of false-positive attached microposts that are actually free microposts. Weakly deflected microposts that are attached to cells are not flagged with this method, so the second scheme uses fluorescence intensity of the GFP expression in cells. The program labels microposts in the "tip post" images as "attached" if they co-localize with pixels in the "cell" images that are within the fluorescently labeled cell. To calculate the strain energy on each attached micropost, the difference between the registered tip and base centroids is squared and multiplied by one-half times the spring constant of a micropost, which is 7.22 nN/μm. mPADs with this spring constant can measure forces in the range of 0.4–36 nN, or 0.01–90 fJ, per micropost. The lower limit is derived from the average deflection of free microposts after registration, which is 0.05 μm. The upper limit is obtainable as a micropost can deflect 5 μm in certain directions without colliding with adjacent posts. Total strain energy per cell was quantified by summing up the strain energies on all attached posts.

Cluster Analysis

To identify patterns in the dynamics of the cellular contractile responses to VEGF stimulation, hierarchical cluster analysis was used to compare how well the dynamics of individual cells correlated [41]. Briefly, Pearson's correlation coefficients were calculated for all pairs of cells that were stimulated with VEGF. The pair with the highest coefficient was clustered by averaging their values, and removing one cell from the data set. This process was iterated until the highest remaining coefficient fell below some minimum value. Otherwise, all cells in the data set would eventually be grouped into the same cluster. As this method can yield markedly different clusters based on which time points of the contractile responses are compared, different observation windows, ranging from the entire 45 minute imaging period to 10–15 minute segments, were used to compute the percentage of cells clustered as a function of the minimum Pearson's correlation coefficient. The observation window with the highest minimum Pearson's correlation coefficient that led to 90% of the cells being clustered was chosen for clustering.

Supplementary Material

Refer to Web version on PubMed Central for supplementary material.

Acknowledgments

The authors would like to thank Zhijun Liu for helpful discussions. This work was supported by NIH grant HL090747. M.T.Y. was partially supported by the National Science Foundation IGERT program (DGE-0221664). The M.I.T. Microsystems Technology Laboratories is acknowledged for support in cleanroom fabrication.

Abbreviations

mPADs	micropost array detectors
PDMS	polydimethylsiloxane
S1P	sphingosine-1-phosphate
BSA	bovine serum albumin
LPA	lysophosphatidic acid
VEGF	vascular endothelial growth factor
FBS	fetal bovine serum
HUVEC	human umbilical vein endothelial cell
MLC	myosin light chain 2
ppMLC	phospho-myosin light chain 2 (Thr18/Ser19)
PBS	phosphate-buffered saline
GFP	green fluorescent protein
DMSO	dimethyl sulfoxide

References

1. Chen CS, Tan J, Tien J. Mechanotransduction at cell-matrix and cell-cell contacts. Annu Rev Biomed Eng. 2004; 6:275–302. [PubMed: 15255771]
2. Chen CS, Mrksich M, Huang S, Whitesides GM, Ingber DE. Geometric control of cell life and death. Science. 1997; 276:1425–8. [PubMed: 9162012]
3. McBeath R, Pirone DM, Nelson CM, Bhadriraju K, Chen CS. Cell shape, cytoskeletal tension, and RhoA regulate stem cell lineage commitment. Dev Cell. 2004; 6:483–95. [PubMed: 15068789]
4. Lauffenburger DA, Horwitz AF. Cell migration: a physically integrated molecular process. Cell. 1996; 84:359–69. [PubMed: 8608589]
5. Wozniak MA, Chen CS. Mechanotransduction in development: a growing role for contractility. Nat Rev Mol Cell Biol. 2009; 10:34–43. [PubMed: 19197330]
6. Burridge K, Chrzanowska-Wodnicka M. Focal adhesions, contractility, and signaling. Annu Rev Cell Dev Biol. 1996; 12:463–518. [PubMed: 8970735]
7. Chrzanowska-Wodnicka M, Burridge K. Rho-stimulated contractility drives the formation of stress fibers and focal adhesions. J Cell Biol. 1996; 133:1403–15. [PubMed: 8682874]
8. Discher DE, Janmey P, Wang YL. Tissue cells feel and respond to the stiffness of their substrate. Science. 2005; 310:1139–43. [PubMed: 16293750]
9. Choquet D, Felsenfeld DP, Sheetz MP. Extracellular matrix rigidity causes strengthening of integrin-cytoskeleton linkages. Cell. 1997; 88:39–48. [PubMed: 9019403]
10. Galbraith CG, Yamada KM, Sheetz MP. The relationship between force and focal complex development. J Cell Biol. 2002; 159:695–705. [PubMed: 12446745]
11. Engler A, Bacakova L, Newman C, Hategan A, Griffin M, Discher D. Substrate compliance versus ligand density in cell on gel responses. Biophys J. 2004; 86:617–28. [PubMed: 14695306]
12. Engler AJ, Sen S, Sweeney HL, Discher DE. Matrix elasticity directs stem cell lineage specification. Cell. 2006; 126:677–89. [PubMed: 16923388]
13. Sniadecki NJ, Anguelouch A, Yang MT, Lamb CM, Liu Z, Kirschner SB, Liu Y, Reich DH, Chen CS. Magnetic microposts as an approach to apply forces to living cells. Proc Natl Acad Sci U S A. 2007; 104:14553–8. [PubMed: 17804810]
14. Yang MT, Sniadecki NJ, Chen CS. Geometric considerations of micro- to nanoscale elastomeric post arrays to study cellular traction forces. Advanced Materials. 2007; 19:3119–3123.

15. Fu JP, Wang YK, Yang MT, Desai RA, Yu XA, Liu ZJ, Chen CS. Mechanical regulation of cell function with geometrically modulated elastomeric substrates. Nature Methods. 2010; 7:733–NIL_95. [PubMed: 20676108]

16. du Roure O, Saez A, Buguin A, Austin RH, Chavrier P, Silberzan P, Ladoux B. Force mapping in epithelial cell migration. Proc Natl Acad Sci U S A. 2005; 102:2390–5. [PubMed: 15695588]

17. Bhadriraju K, Yang M, Alom Ruiz S, Pirone D, Tan J, Chen CS. Activation of ROCK by RhoA is regulated by cell adhesion, shape, and cytoskeletal tension. Exp Cell Res. 2007; 313:3616–23. [PubMed: 17673200]

18. Wojciak-Stothard B, Ridley AJ. Rho GTPases and the regulation of endothelial permeability. Vascul Pharmacol. 2002; 39:187–99. [PubMed: 12747959]

19. Goeckeler ZM, Wysolmerski RB. Myosin light chain kinase-regulated endothelial cell contraction: the relationship between isometric tension, actin polymerization, and myosin phosphorylation. J Cell Biol. 1995; 130:613–27. [PubMed: 7622562]

20. Moy AB, Van Engelenhoven J, Bodmer J, Kamath J, Keese C, Giaever I, Shasby S, Shasby DM. Histamine and thrombin modulate endothelial focal adhesion through centripetal and centrifugal forces. J Clin Invest. 1996; 97:1020–7. [PubMed: 8613524]

21. Vouret-Craviari V, Boquet P, Pouyssegur J, Van Obberghen-Schilling E. Regulation of the actin cytoskeleton by thrombin in human endothelial cells: role of Rho proteins in endothelial barrier function. Mol Biol Cell. 1998; 9:2639–53. [PubMed: 9725917]

22. Carbajal JM, Gratrix ML, Yu CH, Schaeffer RC Jr. ROCK mediates thrombin's endothelial barrier dysfunction. Am J Physiol Cell Physiol. 2000; 279:C195–204. [PubMed: 10898731]

23. van Nieuw Amerongen GP, van Delft S, Vermeer MA, Collard JG, van Hinsbergh VW. Activation of RhoA by thrombin in endothelial hyperpermeability: role of Rho kinase and protein tyrosine kinases. Circ Res. 2000; 87:335–40. [PubMed: 10948069]

24. Wojciak-Stothard B, Potempa S, Eichholtz T, Ridley AJ. Rho and Rac but not Cdc42 regulate endothelial cell permeability. J Cell Sci. 2001; 114:1343–55. [PubMed: 11257000]

25. Liu ZJ, Tan JL, Cohen DM, Yang MT, Sniadecki NJ, Ruiz SA, Nelson CM, Chen CS. Mechanical tugging force regulates the size of cell-cell junctions. Proceedings of the National Academy of Sciences of the United States of America. 2010; 107:9944–9949.10.1073/pnas.0914547107 [PubMed: 20463286]

26. van Nieuw Amerongen GP, Vermeer MA, van Hinsbergh VW. Role of RhoA and Rho kinase in lysophosphatidic acid-induced endothelial barrier dysfunction. Arterioscler Thromb Vasc Biol. 2000; 20:E127–33. [PubMed: 11116077]

27. Essler M, Retzer M, Bauer M, Heemskerk JW, Aepfelbacher M, Siess W. Mildly oxidized low density lipoprotein induces contraction of human endothelial cells through activation of Rho/Rho kinase and inhibition of myosin light chain phosphatase. J Biol Chem. 1999; 274:30361–4. [PubMed: 10521411]

28. Garcia JG, Liu F, Verin AD, Birukova A, Dechert MA, Gerthoffer WT, Bamberg JR, English D. Sphingosine 1-phosphate promotes endothelial cell barrier integrity by Edg-dependent cytoskeletal rearrangement. J Clin Invest. 2001; 108:689–701. [PubMed: 11544274]

29. Vouret-Craviari V, Bourcier C, Boulter E, van Obberghen-Schilling E. Distinct signals via Rho GTPases and Src drive shape changes by thrombin and sphingosine-1-phosphate in endothelial cells. J Cell Sci. 2002; 115:2475–84. [PubMed: 12045218]

30. Moy AB, Blackwell K, Kamath A. Differential effects of histamine and thrombin on endothelial barrier function through actin-myosin tension. Am J Physiol Heart Circ Physiol. 2002; 282:H21–9. [PubMed: 11748043]

31. Hirase T, Kawashima S, Wong EY, Ueyama T, Rikitake Y, Tsukita S, Yokoyama M, Staddon JM. Regulation of tight junction permeability and occludin phosphorylation by Rhoa-p160ROCK-dependent and -independent mechanisms. J Biol Chem. 2001; 276:10423–31. [PubMed: 11139571]

32. Ferrara N, Gerber HP, LeCouter J. The biology of VEGF and its receptors. Nat Med. 2003; 9:669–76. [PubMed: 12778165]

33. Soga N, Namba N, McAllister S, Cornelius L, Teitelbaum SL, Dowdy SF, Kawamura J, Hruska KA. Rho family GTPases regulate VEGF-stimulated endothelial cell motility. Exp Cell Res. 2001; 269:73–87. [PubMed: 11525641]
34. Liu F, Verin AD, Wang P, Day R, Wersto RP, Chrest FJ, English DK, Garcia JG. Differential regulation of sphingosine-1-phosphate- and VEGF-induced endothelial cell chemotaxis. Involvement of G(ialpha2)-linked Rho kinase activity. Am J Respir Cell Mol Biol. 2001; 24:711–9. [PubMed: 11415936]
35. Zeng H, Zhao D, Mukhopadhyay D. KDR stimulates endothelial cell migration through heterotrimeric G protein Gq/11-mediated activation of a small GTPase RhoA. J Biol Chem. 2002; 277:46791–8. [PubMed: 12244099]
36. van Nieuw Amerongen GP, Koolwijk P, Versteilen A, van Hinsbergh VW. Involvement of RhoA/Rho kinase signaling in VEGF-induced endothelial cell migration and angiogenesis in vitro. Arterioscler Thromb Vasc Biol. 2003; 23:211–7. [PubMed: 12588761]
37. Le Boeuf F, Houle F, Sussman M, Huot J. Phosphorylation of focal adhesion kinase (FAK) on Ser732 is induced by rho-dependent kinase and is essential for proline-rich tyrosine kinase-2-mediated phosphorylation of FAK on Tyr407 in response to vascular endothelial growth factor. Mol Biol Cell. 2006; 17:3508–20. [PubMed: 16760434]
38. Tan JL, Tien J, Pirone DM, Gray DS, Bhadriraju K, Chen CS. Cells lying on a bed of microneedles: An approach to isolate mechanical force. Proceedings of the National Academy of Sciences of the United States of America. 2003; 100:1484–1489. [PubMed: 12552122]
39. Sellers JR. Regulation of cytoplasmic and smooth muscle myosin. Curr Opin Cell Biol. 1991; 3:98–104. [PubMed: 1854490]
40. Adelstein RS, Conti MA. Phosphorylation of platelet myosin increases actin-activated myosin ATPase activity. Nature. 1975; 256:597–8. [PubMed: 170529]
41. Eisen MB, Spellman PT, Brown PO, Botstein D. Cluster analysis and display of genome-wide expression patterns. Proc Natl Acad Sci U S A. 1998; 95:14863–8. [PubMed: 9843981]
42. Lampugnani MG, Orsenigo F, Gagliani MC, Tacchetti C, Dejana E. Vascular endothelial cadherin controls VEGFR-2 internalization and signaling from intracellular compartments. J Cell Biol. 2006; 174:593–604. [PubMed: 16893970]
43. Sawamiphak S, Seidel S, Essmann CL, Wilkinson GA, Pitulescu ME, Acker T, Acker-Palmer A. Ephrin-B2 regulates VEGFR2 function in developmental and tumour angiogenesis. Nature. 465:487–91. [PubMed: 20445540]
44. Caswell PT, Vadrevu S, Norman JC. Integrins: masters and slaves of endocytic transport. Nat Rev Mol Cell Biol. 2009; 10:843–53. [PubMed: 19904298]
45. Ezratty EJ, Bertaux C, Marcantonio EE, Gundersen GG. Clathrin mediates integrin endocytosis for focal adhesion disassembly in migrating cells. J Cell Biol. 2009; 187:733–47. [PubMed: 19951918]
46. Soldi R, Mitola S, Strasly M, Defilippi P, Tarone G, Bussolino F. Role of alphavbeta3 integrin in the activation of vascular endothelial growth factor receptor-2. Embo J. 1999; 18:882–92. [PubMed: 10022831]
47. Becker PM, Verin AD, Booth MA, Liu F, Birukova A, Garcia JG. Differential regulation of diverse physiological responses to VEGF in pulmonary endothelial cells. Am J Physiol Lung Cell Mol Physiol. 2001; 281:L1500–11. [PubMed: 11704547]
48. Zemel A, Rehfeldt F, Brown AE, Discher DE, Safran SA. Optimal matrix rigidity for stress fiber polarization in stem cells. Nat Phys. 6:468–473. [PubMed: 20563235]
49. Otsu N. Threshold Selection Method from Gray-Level Histograms. Ieee Transactions on Systems Man and Cybernetics. 1979; 9:62–66.
50. Lemmon CA, Sniadecki NJ, Ruiz SA, Tan JL, Romer LH, Chen CS. Shear force at the cell-matrix interface: enhanced analysis for microfabricated post array detectors. Mech Chem Biosyst. 2005; 2:1–16. [PubMed: 16708468]

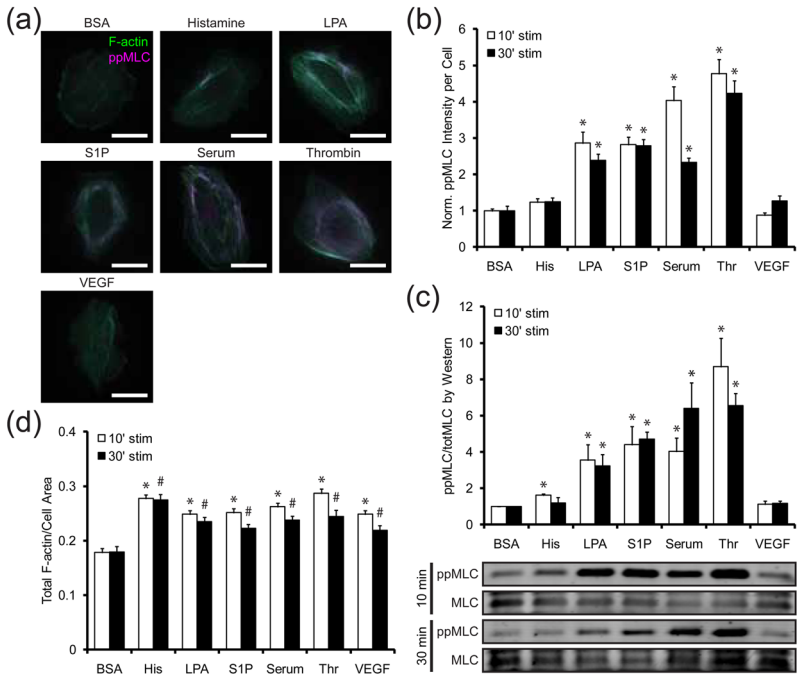

Figure 1. Effects of vasoactive agonists on actin organization and myosin activity

(a) Representative images of cells stimulated with BSA (10 μg/mL), histamine (3 μM), LPA (10 μg/mL), S1P (0.5 μM), serum (20% v/v FBS), thrombin (1 U/mL), or VEGF (50 ng/mL) for 10 min. F-actin (green) and ppMLC (magenta) are labeled. Scale bars are 25 μm. **(b)** Fold change in ppMLC immunofluorescence in cells stimulated with BSA (10 μg/mL), histamine (His; 3 μM), LPA (10 μg/mL), S1P (0.5 μM), serum (20% v/v FBS), thrombin (Thr; 1 U/mL), or VEGF (50 ng/mL) for 10 (white bars) and 30 (black bars) min. ppMLC is normalized to the BSA treatment condition for each stimulation duration. Data for each treatment condition is the average of n = 20 cells from one experiment. Error bars indicate SEM. * $p < 0.001$ indicates comparison against BSA control for the respective stimulation duration. **(c)** Fold change in ppMLC immunoblot intensity in cells stimulated with the same treatment conditions in (b) for 10 (white bars) and 30 (black bars) min. ppMLC is first normalized against total MLC expression and then normalized to the BSA treatment condition. Data is the average of three independent experiments. Error bars indicate SEM. * $p < 0.1$ indicates comparison against BSA control for the respective stimulation duration. **(d)** Fractional coverage of F-actin in cells stimulated with the same treatment conditions in (b) for 10 (white bars) and 30 (black bars) min. Data for each treatment condition is the average of n = 20 cells from one experiment. Error bars indicate SEM. * $p \ll 0.001$ indicates comparison against BSA control for 10 min stimulation. # $p < 0.01$ indicates comparison against BSA control for 30 min stimulation.

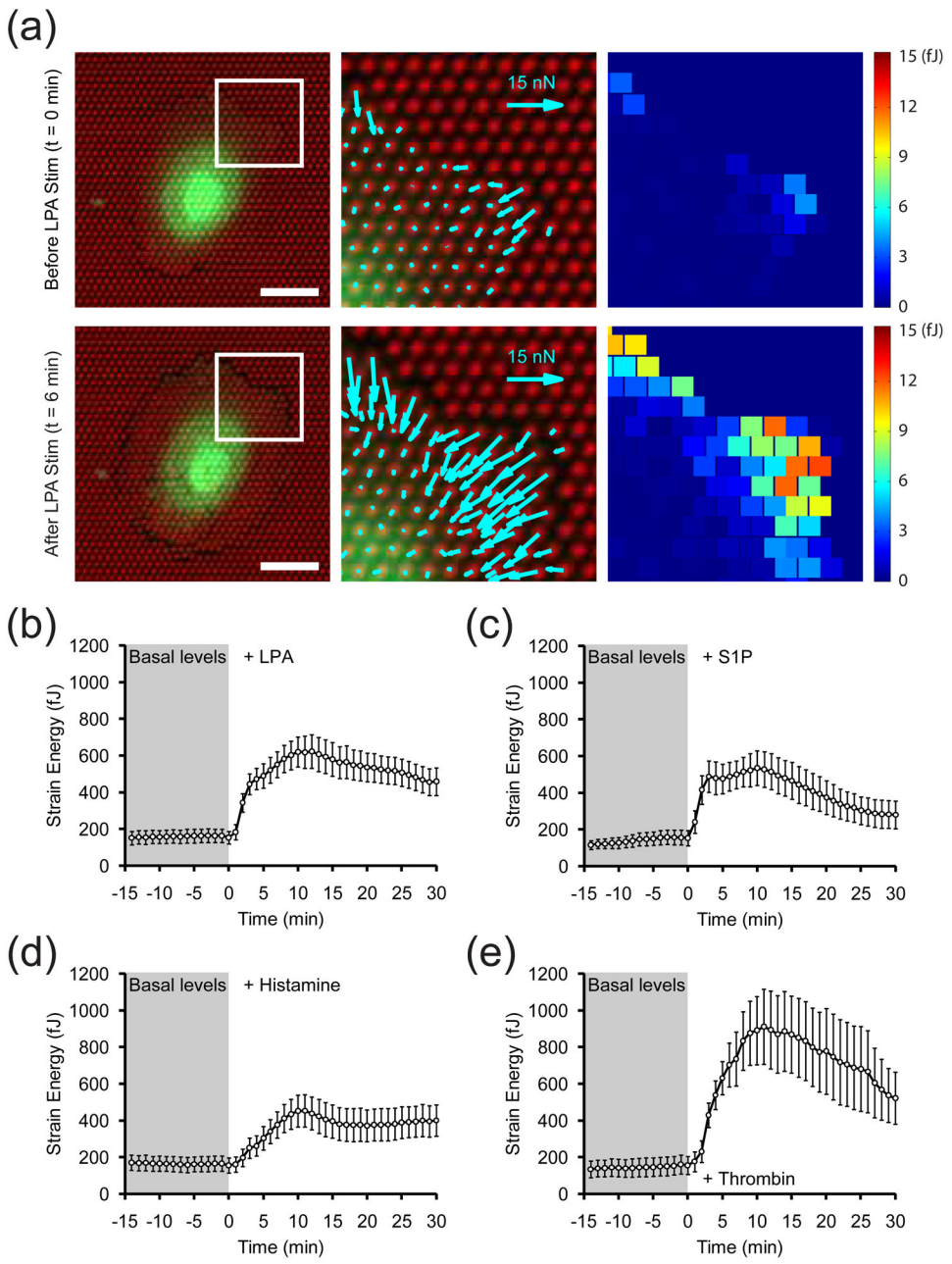

Figure 2. Effects of vasoactive agonists on contractility

(a) Traction force and strain energy maps of a representative cell before (top row) and after (bottom row) stimulation with LPA (10 μg/mL). The insets in the left panels are magnified in the middle and right panels, which show the traction force vectors and strain energy magnitudes, respectively. Scale bars are 30 μm. **(b–e)** Time-series plots of the average strain energy of cells stimulated with **(b)** LPA (10 μg/mL), **(c)** S1P (0.5 μM), **(d)** histamine (3 μM) or **(e)** thrombin (10 nM) immediately after t = 0 min. Data for each treatment condition is the average of n = 17 (LPA), n = 16 (S1P), n = 16 (histamine), and n = 11 (thrombin) cells from one experiment each. Error bars are ± SEM.

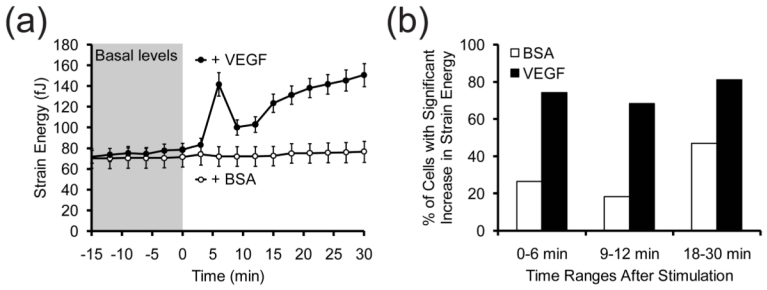

Figure 3. Effect of VEGF on contractility

(a) Time-series plot of the average strain energy of cells stimulated with BSA (white circles, 10 μg/mL) or VEGF (black circles, 50 ng/mL) immediately after t = 0 min. Data for each treatment condition is the average of n = 49 (BSA) and n = 85 (VEGF) cells pooled from at least three experiments each. Error bars are ± SEM. **(b)** Percentages of cells in (a) that had significant ($p < 0.05$) increases in strain energy at early (0–6 min), intermediate (9–12 min) and late (18–30 min) time periods following addition of BSA (white bars) or VEGF (black bars). For early and intermediate time periods, the Student's t-test was used to compare single time points in the respective time ranges against 6 basal time points from t = −15 to 0 min. For late time periods, all time points between t = 18 to 30 min were compared against the 6 basal time points.

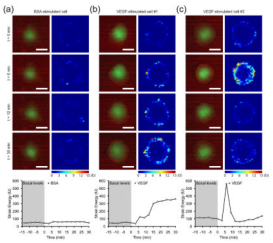

Figure 4. Single-cell heterogeneity in the VEGF-induced contractile response

(a–c) Time-series images of three representative GFP-expressing cells on mPADs, stimulated with BSA (10 μg/mL) or VEGF (50 ng/mL) immediately after t = 0 min. The corresponding colorimetric map of the strain energy on each micropost is shown next to each image of the cell. The time-series plot of total strain energy for each representative cell is shown below the respective images. Scale bars are 30 μm.

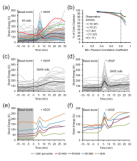

Figure 5. Cluster analysis of VEGF-induced contractility dynamics

(a) Time-series plot of the strain energy profiles of individual cells that were stimulated with VEGF (50 ng/mL) immediately after t = 0 min. 85 cells, pooled from four experiments, are plotted with selected cells highlighted in color. **(b)** Determination of the optimal window of the observation period to use for hierarchical clustering. Pearson correlation coefficients were computed using time points from 15 minutes pre-stimulation to 30 minutes post-simulation (−15′,30′), (−15′,0′), (1′,30′), (11′,30′), and (1′,11′). The percentage of cells clustered is plotted as a function of the minimum Pearson correlation coefficient allowed. Using the (1′,11′) window results in the highest percentage of clustered cells at a minimum Pearson correlation coefficient of 0.8 (dotted line). **(c–d)** Time-series plot of the two largest clusters parsed from the data in (a). The (1′,11′) window and a minimum Pearson correlation coefficient of 0.8 were used to cluster strain energy profiles. The cluster in **(c)** consists of 25 cells that lack a spike in strain energy. The cluster in **(d)** consists of 39 cells that experience a spike in strain energy at t = 6 min. The bold black line is the average while gray lines represent individual cells. The remaining 21 cells were classified into much smaller clusters (not shown). **(e)** Time-series plot of the average strain energies of cells in (a) grouped by their basal contractility. The 85 observed cells were split into 5 groups of 17 cells based on a percentile calculation of their average basal strain energy between t = −15 and 0 min (gray box). The percentile ranges are color-coded in the legend. **(f)** Time-series plot of the average strain energies of cells in (a) grouped by their initial spread area. The 85 observed cells were split into 5 groups of 17 cells based on a percentile calculation of their cell area at t = 0 min (gray box). The percentile ranges are color-coded in the legend.

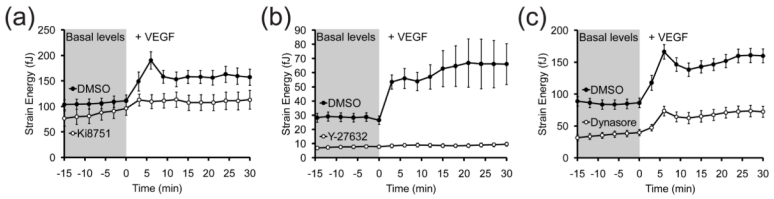

Figure 6. Effects of VEGFR2, ROCK and dynamin inhibition on the VEGF-induced contractile response

(a) Time-series plot of the average strain energy of cells pre-treated with 10 μM Ki8751 (white circles) or DMSO (black circles) from t = −60 to 0 min and then stimulated with VEGF (50 ng/mL) immediately after t = 0 min. Data for each treatment condition is the average of n = 23 (Ki8751 + VEGF) and n = 47 (DMSO + VEGF) cells from one and two experiments, respectively. Error bars are ± SEM. **(b)** Time-series plot of the average strain energy of cells pre-treated with 25 μM Y-27632 (white circles) or DMSO (black circles) from t = −30 to 0 min and then stimulated with VEGF (50 ng/mL) immediately after t = 0 min. Data for each treatment condition is the average of n = 26 (Y-27632 + VEGF) and n = 58 (DMSO + VEGF) cells from two and four experiments, respectively. Error bars are ± SEM. **(c)** Time-series plot of the average strain energy of cells pre-treated with 30–50 μM Dynasore (white circles) or DMSO (black circles) from t = −60 to 0 min and then stimulated with VEGF (50 ng/mL) immediately after t = 0 min. Data for each treatment condition is the average of n = 95 (Dynasore + VEGF) and n = 96 (DMSO + VEGF) cells from four experiments each. Error bars are ± SEM.

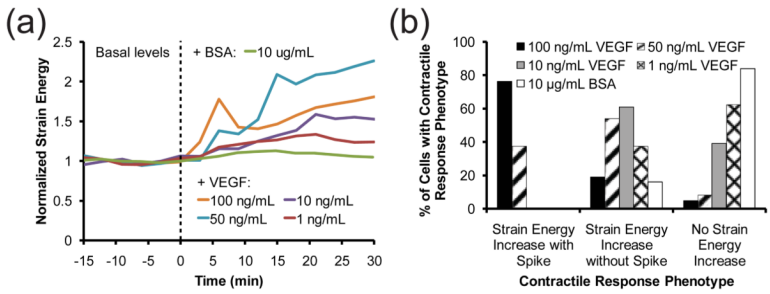

Figure 7. Dose-dependent effects of VEGF on contractility

(a) Time-series plot of the average normalized strain energy of cells stimulated with BSA or different concentrations of VEGF (indicated in the legend) immediately after t = 0 min. The strain energies of individual cells were normalized to their average basal levels from t = −15 to 0 min. Averages represent 21–25 cells per treatment condition from one experiment. **(b)** Percentages of cells in (a) that responded to BSA or different concentrations of VEGF (indicated in the legend) with one of three contractile phenotypes: an increase in strain energy with a contractile spike, an increase in strain energy without a spike, or no increase in strain energy.

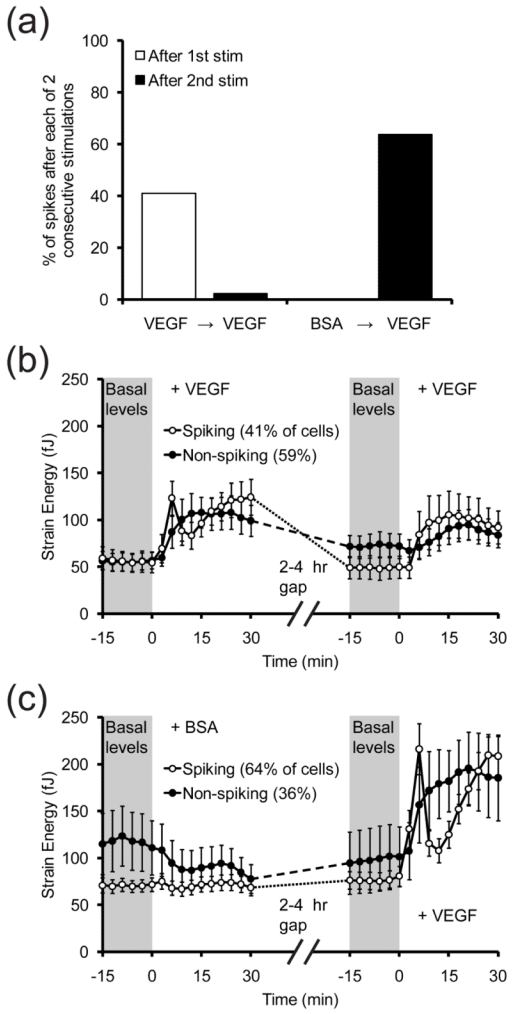

Figure 8. Effects of repeated stimulations of VEGF on contractility

(a) Bar graph showing the percentage of cells that spike after two stimulations. VEGF (50 ng/mL) or BSA (10 μg/mL) is administered first, and after 2–4 hours, VEGF (50 ng/mL) is added again. Cells were starved in EBM-2 before and in-between stimulations. **(b)** Time-series plot of the average strain energy of cells that have been stimulated with VEGF twice as described in (a). Strain energy is measured over two 45-minute observation periods for the first and second stimulations, which are added immediately after t = 0 min. Cells were grouped based on whether they spiked (white circles) or did not spike (black circles) after the first stimulation. n = 44 cells pooled from two experiments. Error bars are ± SEM. **(c)** Time-series plot of the average strain energy of cells that have been stimulated with BSA followed by VEGF as described in (a). Cells were starved in EBM-2 before and in-between stimulations. Strain energy is measured over two 45-minute observation periods for the first and second stimulations, which are added immediately after t = 0 min. Cells were grouped based on whether they spiked (white circles) or did not spike (black circles) after the second stimulation. n = 44 cells pooled from two experiments. Error bars are ± SEM.